

# XQ-GAN: An Open-source Image Tokenization Framework for Autoregressive Generation

Xiang Li<sup>1\*</sup>, Kai Qiu<sup>1\*</sup>, Hao Chen<sup>1</sup>, Jason Kuen<sup>2</sup>, Jiuxiang Gu<sup>2</sup>, Jindong Wang<sup>3</sup>, Zhe Lin<sup>2</sup>, Bhiksha Raj<sup>1</sup>  
<sup>1</sup>Carnegie Mellon University, <sup>2</sup>Adobe Research, <sup>3</sup>William & Mary

Quantization	Reference	Backbone	Reference	Alignment	Reference
Vector Quant. (VQ)	VQVAE [62]	CNN	VQGAN [12]	DINO-v2	ImageFolder [30]
Residual Quant. (RQ)	RQVAE [26]	Transformer	ImageFolder [30]	CLIP	VILA-U [67]
Product Quant. (PQ)	ImageFolder [30]	Discriminator	Reference	Pre-training	Reference
Look-up Free Quant. (LFQ)	MAGVIT-v2 [74]	StyleGAN	StyleGAN [22]	ImageNet	ImageNet [7]
Binary Spherical Quant. (BSQ)	BSQ-ViT [80]	PatchGAN	PatchGAN [21]	LAION-400M	LAION-400M [51]
Multi-Scale RQ (MSRQ)	VAR [57]	DINO	VAR [57]	IMed-361M	IMed-361M [5]

Table 1. Overview of XQ-GAN components and their design choices. The framework consists of five main components: Encoder, Decoder, Quantization, Semantic alignment, and Discriminator, each offering multiple design choices for exploration. We provide pre-trained weights on several datasets and support fine-tuning with full parameters, LORA [19] and frozen encoder/decoder.

## Abstract

*Image tokenizers play a critical role in shaping the performance of subsequent generative models. Since the introduction of VQ-GAN, discrete image tokenization has undergone remarkable advancements. Improvements in architecture, quantization techniques, and training recipes have significantly enhanced both image reconstruction and the downstream generation quality. In this paper, we present XQ-GAN, an image tokenization framework designed for both image reconstruction and generation tasks. Our framework integrates state-of-the-art quantization techniques, including vector quantization (VQ), residual quantization (RQ), multi-scale residual quantization (MSVQ), product quantization (PQ), lookup-free quantization (LFQ), and binary spherical quantization (BSQ), within a highly flexible and customizable training environment. On the standard ImageNet 256×256 benchmark, our released model achieves an rFID of 0.64, significantly surpassing MAGVIT-v2 (0.9 rFID) and VAR (0.9 rFID). Furthermore, we demonstrate that using XQ-GAN as a tokenizer improves gFID metrics alongside rFID. For instance, with the same VAR architecture, XQ-GAN+VAR achieves a gFID of 2.6, outperforming VAR’s 3.3 gFID by a notable margin. To support further research, we provide pre-trained weights of different image tokenizers for the community to directly train the subsequent generative models on it or fine-tune for specialized tasks.*

<https://github.com/1xa9867/ImageFolder>

## 1. Introduction

Autoregressive (AR) image generation [31, 57, 66, 67] has achieved notable progress and demonstrated promising per-

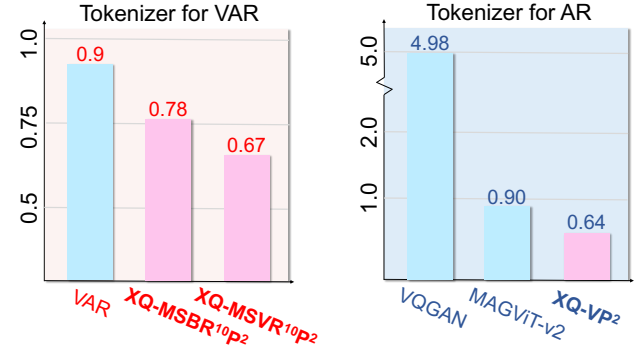


Figure 1. Performance comparison of XQGAN and prior arts on ImageNet 256x256 reconstruction benchmark. We provide XQGAN’s tokenizer for vanilla AR and VAR [57] modeling. Our proposed XQGAN demonstrates superior performance against mainstream tokenizers for both AR and VAR tasks. XQ-GAN variants are named with XQ- {multi-scale (MS)}-{vector quantization (V), lookup free quantization (L), binary spherical quantization (B)}-{residual quantization (R)}<sup>N</sup>-{product quantization (P)}<sup>P</sup> where N and P denotes residual depth and product branch number respectively.

formance recently. The current advanced image generation paradigm typically requires a pre-trained image tokenizer [12, 30, 73, 74, 76] that encodes the image into a more compact latent space, where an AR generator, e.g. vision transformer [1], is leveraged to model the latent distribution, for both efficiency and effectiveness in generation [47].

Recent approaches [30, 55, 67] demonstrate that the construction of latent space has a significant impact on the subsequent image generation quality. Different variables, such as token number [30, 55], semantics [30, 57, 67] and code-

book utilization [70, 74, 83] have been shown to significantly affect the generation quality in previous research.

For AR generation, the quantization approaches are vital to learn the latent representation. VQVAE [62] introduces a vector quantization (VQ) approach by leveraging the idea of the nearest neighbor to encode continuous tokens into a finite set of discrete tokens. After that, residual quantization (RQ) [26] and multi-scale residual quantization (MSRQ) [57] are further proposed to hierarchically quantize the continuous tokens. More recently, product quantization [30] (PQ) is introduced to separate the continuous space into several smaller subspaces and separately quantize them. Look-up free quantization (LFQ) [74] and its improved version binary spherical quantization (BSQ) [80] addressed the codebook utilization issue when handling large codebook size.

Recent studies [30, 77] also indicate that a semantic-rich representation can substantially benefit the generation quality. From the tokenizer side, ImageFolder [30] leverages DINO-v2 [39] to inject semantics into the product quantized tokens. Similarly, VILA-U [67] utilizes CLIP [43] to enhance the semantics of image tokens for unified understanding and generation using a large language model (LLM). SoftVQ-VAE [15] explores several different semantic alignment combinations and manages to achieve a highly compact representation, i.e., 32 tokens, for both reconstruction and generation. However, there is no unified framework for training tokenizers and subsequent generation tasks with different techniques proposed in previous methods.

In this paper, we propose XQ-GAN, an open-source and highly customizable framework for image tokenization and subsequent generation. The proposed framework presents several advantages over the previous ones [33, 55].

- As shown in Tab. 1, XQ-GAN provides implementations of various quantization approaches, encoder and decoder backbones, discriminator architectures, and semantic alignment approaches, thus permitting a modular and flexible combination of them.
- To further facilitate the community, we provide several pre-trained weights on large-scale datasets, such as ImageNet [7] (1000-class natural image), LAION-400M [51] (text-rich natural image) and IMed-361M [5] (14 categories, multimodal medical image).
- Following the standard benchmarking setting, we benchmark our framework on several settings. Notably, the best performance of the proposed XQ-GAN significantly outperforms the previous counterparts MAGVIT-v2 and VAR by a large margin.

## 2. Related Works

### 2.1. Image Tokenizers

Image tokenizer has seen significant progress in multiple image-related tasks. Traditionally, autoencoders [18, 64]

have been used to compress images into latent spaces for downstream work such as (1) generation and (2) understanding. In the case of generation, VAEs [45, 62] learn to map images to probabilistic distributions; VQGAN [12, 46] and its subsequent variants [20, 25, 33, 34, 56, 66, 71–73, 81, 83, 85] introduce a discrete latent space for better compression for generation. On the other hand, understanding tasks, such as CLIP [43], DINO [6, 39, 86], rely heavily on LLM [11, 63] to tokenize images into semantic representations [10, 38]. These representations are effective for tasks like classification [11], object detection [84], segmentation [65], and multi-modal application [69]. For a long time, image tokenizers have been divided between methods tailored for generation and those optimized for understanding. After the appearance of [75], which proved the feasibility of using LLM as a tokenizer for generation, some works [67] are dedicated to unify the tokenizer for generation and understanding due to the finding in [14].

### 2.2. Autoregressive Visual Generation

Autoregressive models have shown remarkable success in generating high-quality images by modeling the distribution of pixels or latent codes in a sequential manner. Early autoregressive models such as PixelCNN [61] pioneered the approach of predicting pixel values conditioned on previously generated pixels. The transformer architecture [63], first proposed in NLP, has spread rapidly to image generation [35, 52] because of its scalability and efficiency. MaskGIT [4] accelerated the generation by predicting tokens in parallel, while MAGE [28] applied MLLM [3, 41] to unify the visual understanding and the generation task. Recently, autoregressive models continued to show their scalability power in larger datasets and multimodal tasks [16]; models like LlamaGen [55] adapting Llama [58] architectures for image generation. New directions such as VAR [31, 57], MAR [29] and Mamba [27] have further improved flexibility and efficiency in image synthesis. Currently, more and more unified multimodal models like SHOW-O [68], Transfusion [82] and Lumina-mGPT [32] continue to push the boundaries of autoregressive image generation, demonstrating scalability and efficiency in diverse visual tasks.

### 2.3. Diffusion Models for Image Generation

Diffusion models, initially introduced by Sohl-Dickstein et al. [53] as a generative process and later expanded into image generation by progressively infusing fixed Gaussian noise into an image as a forward process. A model, such as U-Net [49], is then employed to learn the reverse process, gradually denoising the noisy image to recover the original data distribution. In recent years, this method has witnessed significant advancements driven by various research efforts. Nichol et al. [36], Dhariwal et al. [8],

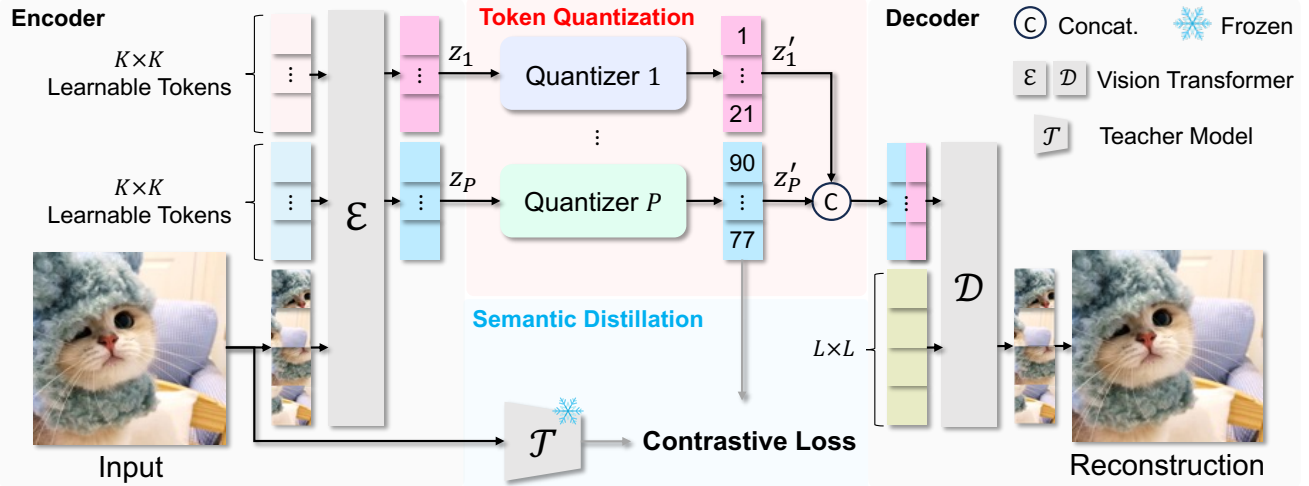


Figure 2. Overview of XQ-GAN-SC pipeline with latent spatial compression (SC). In this pipeline, a vision transformer is adopted as the encoder and decoder.  $P$  set of  $K \times K$  learnable tokens are utilized as queries to query the image tokens.  $P$  denotes the quantizer number where  $P = 1$  is the vanilla Vector Quantization [12] setting and  $P > 1$  denotes a Product Quantization [30] setting.  $K \times K$  denotes the spatial resolution of the quantized latent. During decoding,  $L \times L$  learnable tokens are leveraged to query the quantized tokens and then decoded to the reconstructed image. The cost of image decoding is independent to the quantizer number, making it suitable for generation tasks that only require decoding during inference.

and Song et al. [54] proposed various techniques to enhance the effectiveness and efficiency of diffusion models, paving the way for improved image generation capabilities. Notably, the paradigm shift towards modeling the diffusion process in the latent space of a pre-trained image encoder as a strong prior [12, 62] rather than in raw pixel spaces [48, 60] has proven to be a more efficient and instrumental method for high-quality image generation. Moreover, a lot of research on the model architecture replaces or integrates the vanilla U-Net with a transformer [40] to further improve the capacity and efficiency of multi-model synthesis on diffusion model. Inspired by these promising advancements in diffusion models, numerous foundational models have emerged, driving innovation in both image quality and flexibility. For instance, Glide [37] introduced a diffusion model for text-guided image generation, combining diffusion techniques with text encoders to control the generated content. Cogview [9] leveraged transformer architectures alongside diffusion methods to enhance image generation tasks. Make-A-Scene [13] and Imagen [50] focused on high-fidelity image synthesis conditioned on textual inputs, showcasing the versatility of diffusion models across modalities. DALL-E [44] and Stable Diffusion [47] brought diffusion models to mainstream applications, demonstrating their ability to generate high-resolution photorealistic images.

### 3. XQ-GAN

XQ-GAN is a customizable framework for advanced image tokenization. Two types of pipelines are implemented

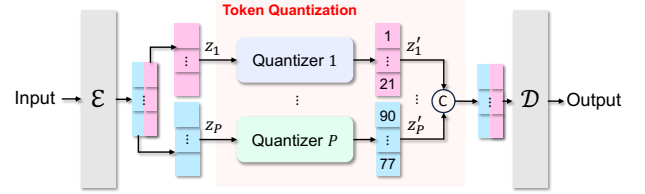


Figure 3. XQ-GAN-V pipeline.

- XQ-GAN-Spatial Compression (SC), for reducing the latent resolution, and XQ-GAN-Vanilla (V), for being compatible with classic tokenizers. Semantic alignment and adversarial discriminators can be further applied to these pipelines.

#### 3.1. XQ-GAN-SC

The XQ-GAN-SC pipeline tokenizes images with three main components - Encoder, Decoder, and Token Quantization module. Following ImageFolder [30], vision transformers are leveraged as the encoder and decoder. As shown in Fig. 2, given an input image  $I$ , we first patchify it into a set of  $L \times L$  tokens where  $L$  is the patch size. After that, the image tokens are concatenated with  $P$  sets of  $K \times K$  learnable tokens and serve as the input to the transformer encoder  $E$ . The same spatial positional encodings are added to the learnable tokens to inform the spatial alignment. A level embedding is additionally used to convey the difference across  $K \times K$  tokens. Let us denote the encoded tokens corresponding to the learnable tokens as  $z_1, \dots, z_P$ . To discretize them, we use different quantizers  $Q_1, \dots, Q_P$  ( $P = 1$  is equivalent to

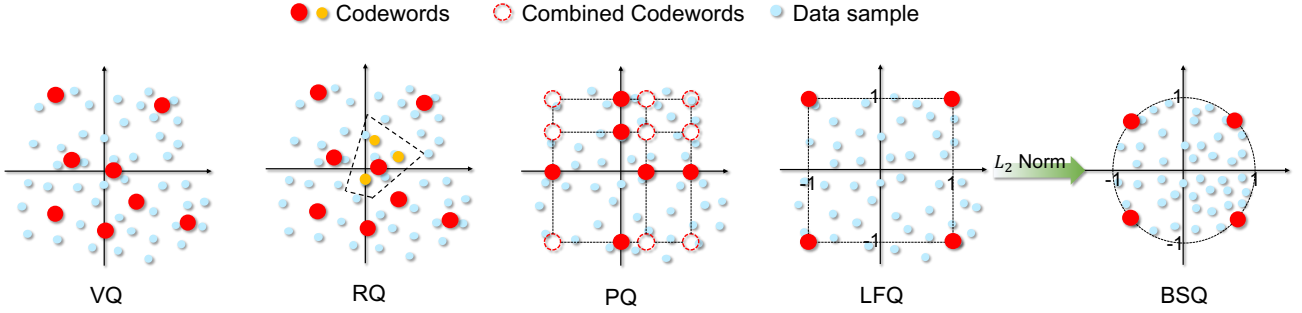


Figure 4. Visualization of Vector Quantization (VQ), Residual Quantization (RQ), Product Quantization (PQ), Lookup Free Quantization (LFQ), and Binary Spherical Quantization (BSQ) in a simple two-dimensional space. VQ equivalent to k-means clustering, partitions the space into Voronoi regions based on the nearest centroids. RQ refines this region iteratively by quantizing residual at each step. PQ quantized the space with the combination of several codewords on subspaces. LFQ projects the tokens into several binary subspaces and quantizes each subspace with  $[-1, 1]$ . BSQ applied an  $L_2$  normalization on LFQ’s subspace prior to quantization, resulting in a spherical quantization boundary.

vanilla VQ). The quantized tokens  $z'_1, \dots, z'_P$  are further concatenated with a set of  $L \times L$  learnable tokens to decode the reconstructed image with a decoder  $\mathcal{D}$ .

### 3.2. XQ-GAN-V

XQ-GAN-V pipeline follows the vanilla VQ-GAN [12] architecture while enhancing the token quantization part to support customizable quantization with different tokenization approaches. Specifically, as shown in Fig. 3, given an input image  $I$ , we extract features with an encoder  $\mathcal{E}$ . After that, the extracted features are channel-wise chunked into several subtokens and separately conduct quantization. The quantized tokens  $z'_1, \dots, z'_P$  are further concatenated and fed to the decoder to reconstruct the image.

## 4. Quantization

To incorporate the combination of different quantization approaches, we propose a hierarchical pipeline. As shown in Fig. 5, XQ-GAN first decides the quantizer number  $P$  for product quantization. After that, each quantizer is assumed to be a residual quantizer where each residual quantizer can be a vector quantizer, look-up free quantizer, or binary spherical quantizer. It is worth noting that, with a  $P = 1, N = 1$ , and VQ as residual quantizer, the framework is equivalent to conducting vanilla VQ proposed in VQGAN [12].

### 4.1. Vector Quantization

Vector quantization (VQ) [12] introduces a learnable codebook that maps continuous input features to discrete latent representations, enabling generative models in a K-means manner. Specifically, each input continuous feature  $x$  was processed with a learned, discrete codebook  $\mathcal{C} = \{e_j\}_{j=1}^J$

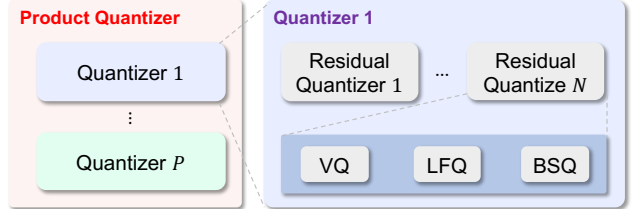


Figure 5. Hierarchical quantizer design. With  $P = 1, N = 1$ , and VQ for residual quantizer, the quantizer is equivalent to the vanilla VQ [12].

by mapping to its closest codeword  $z$  as follow:

$$z' = \arg \min_{e_j \in \mathcal{C}} \|z - e_j\|_2^2 \quad (1)$$

where  $z'$  is the quantized representation of the input.

### 4.2. Residual Quantization

Residual quantization (RQ) [57] leverages multiple tokens  $\hat{z}_1, \hat{z}_2, \dots, \hat{z}_N$  to represent an image, where  $N$  denotes the number of residual steps. In the  $i$ -th residual step, the RQ quantizes the input  $r_i$  by mapping it to its closest vector in the codebook  $\mathcal{C} = \{e_j\}_{j=1}^J$  as  $z'_i = \arg \min_{e_j \in \mathcal{C}} \|r_i - e_j\|_2^2$ . After the nearest-neighbor look-up, the quantized representation  $z'_i$  is subtracted by the input to form a residual representation which serves as the input to the next residual layer:

$$\begin{aligned} z_i &= z_{i-1} - z'_{i-1} \\ r_i &= r_{i-1} - z_i \\ z_0 &= 0 \\ r_0 &= 0 \end{aligned} \quad (2)$$

where  $r$  is the residual.

**Quantizer dropout.** Specifically, to enhance the representation capability, we notice that a quantizer dropout strategy [24, 78] may improve generation performance. During training, quantizer dropout randomly drops out the last several quantizers. The quantizer dropout happens with a ratio of  $p$ . With the quantizer dropout, the final output of the Residual Quantization can be formulated as:

$$z' = \sum_{i=1}^n z'_i, N_{start} \leq n \leq N. \quad (3)$$

Applying quantizer dropout enables residual quantizers to encode images into different bitrates depending on the residual steps.

### 4.3. Product Quantization

Product quantization (PQ) [30] aims to quantize a high-dimension vector to a combination of several low-dimension tokens, which has shown a promising capability to capture different contexts across sub-quantizers [2]. Given a continuous feature  $z$ , product quantization performs as:

$$\mathcal{P}(z) = \mathcal{Q}_1(z_1) \oplus \cdots \oplus \mathcal{Q}_P(z_P), \mathcal{Q}_p \sim \mathcal{C}_p, \quad (4)$$

where  $\oplus$  denotes channel-wise concatenation (cartesian product),  $\sim$  denotes that vector quantizer  $\mathcal{Q}_p$  is associated with the codebook  $\mathcal{C}_p = \{e_j\}_{j=1}^J$ , i.e.,  $\mathcal{Q}_p$  maps a feature  $z_p$  to a codeword  $e_p = \arg \min_{e_j \in \mathcal{C}_p} \|z_p - e_j\|_2^2$  that minimizes the distance between  $z_p$  and  $e_j \in \mathcal{C}_p$ .  $P$  is the product number, i.e., sub-vector number and  $z_p$  is a sub-vector from  $z$  having  $z = \oplus_{p=1}^P z_p$ . Product quantization first divides the target vector into several sub-vectors and then quantizes them separately. After the quantization, the quantized vectors resemble the original vector by concatenation.

### 4.4. Lookup Free Quantization

Lookup-free quantization (LFQ) [71] is a special variant of product quantization that quantizes high-dimension vectors to a combination of several low-dimension tokens. LFQ decomposes the latent space as the Cartesian product of  $\log_2^J$  single-dimensional variables and formulated as  $\mathcal{C} = \times_{p=1}^{\log_2^J} \mathcal{C}_p$  where  $\mathcal{C}_p = \{1, -1\}$  and  $J$  denotes the global codebook size. Given a feature vector  $z \in \mathbb{R}^{\log_2^K}$ , each dimension of the vector  $z[p]$  can be separately quantized by a codebook  $\mathcal{C}_p$ , leading to a binary quantized value for each dimension, i.e., -1 or 1.

### 4.5. Binary Spherical Quantization

Similar to LFQ, binary spherical quantization (BSQ) has recently been proposed to improve its performance. Recall that the feature vector  $z$  is defined in  $\mathbb{R}^{\log_2^K}$ , which may lead to substantial quantization error as  $\mathcal{C}_p = \{-1, 1\}$ . This may

barrier the straight-through gradient backpropagation [15]. In this way, BSQ additionally introduces a  $L_2$  norm upon the feature vector  $z$  to bound the quantization error to  $[0, 1]$ .

### 4.6. Multi-scale Residual Quantization

VAR [57] enhances the vanilla RQ with a multi-scale setting. The feature map  $r_{i-1}$  is first downsampled from its original dimension  $L \times L$  to a lower resolution  $L_i \times L_i$  where  $L_i$  represents the resolution of current residual  $r_i$ . After downsampling, the look-up procedure is performed to match each feature vector with the closest codebook vector. After the look-up, the quantized vector  $z_i$  is upsampled back to the original dimension  $L \times L$  to ensure consistency across scales. Due to the loss of high-frequency information from downsampling, [57] utilized a 2D convolutional layer after upsampling to restore the lost details and enhance the fidelity of the reconstructed image. Specifically, this convolutional layer processes the upsampled feature vectors according to the equation:

$$\hat{z}'_i = \gamma \times \text{conv}(z'_i) + (1 - \gamma) \times z'_i \quad (5)$$

where  $\gamma$  is a constant.

## 5. Semantic Alignment

Recent works [30, 67] indicate the semantic-rich latent space has substantial benefits to the downstream generation qualities.

To impose semantics into the tokenized image representation, we propose a semantic alignment term to the quantized token  $z'$ . A frozen pre-trained **DINOv2** model [39] or **CLIP** [43] can be utilized to extract the semantic-rich visual feature  $f$  of the input image  $I$ . Two types of alignments are supported:

- **Token-level:** The quantized token  $z'$  and visual feature  $f$  are pooled to  $1 \times 1$ .
- **Patch-level:** The quantized token  $z'$  and visual feature  $f$  are resized to the same shape.

A CLIP-style contrastive loss [43] is adopted to perform visual alignment: maximizing the similarity between the quantized tokens  $z'$  and their corresponding DINO representation  $f$ , while minimizing the similarity between  $z'$  and other representations  $f$  from different images within one batch. To facilitate semantic learning, we initialize the image encoder  $\mathcal{E}$  with the same weight as the frozen one if the XQ-GAN-SC pipeline is leveraged.

## 6. Adversarial Discriminator

We provide the interface for different discriminators, i.e., PatchGAN, StyleGAN and DINO, different discriminator losses, i.e., hinge, vanilla, and non-saturating, and different generator losses, i.e., hinge and non-saturating.

Method	RQ	PQ	MS	VQ	LFQ	BSQ	Latent Res.	$ \mathcal{C} $	rFID $\downarrow$	Util. $\uparrow$
Performance without residual quantization										
VQGAN [12]	1	1		✓			$16 \times 16$	16384	4.98	63%
VIT-VQGAN [70]	1	1		✓			$16 \times 16$	4096	1.55	96%
MAGVIT-v2 [74]	1	1			✓		$16 \times 16$	262144	~0.9	100%
XQGAN-VP <sup>2</sup>	1	2		✓			$16 \times 16$	4096	0.94	100%
XQGAN-VP <sup>2</sup>	1	2		✓			$16 \times 16$	16384	<b>0.64</b>	100%
Performance with residual quantization										
RQGAN [26]	4	1		✓			$16 \times 16 \rightarrow 16 \times 16$	16384	1.83	-
VAR [57]	10	1		✓	✓		$1 \times 1 \rightarrow 16 \times 16$	4096	0.90	100%
XQGAN-MSVR <sup>10P<sup>2</sup></sup>	10	2		✓	✓		$1 \times 1 \rightarrow 11 \times 11$	4096	0.80	100%
XQGAN-MSVR <sup>10P<sup>2</sup></sup>	10	2		✓	✓		$1 \times 1 \rightarrow 11 \times 11$	8192	0.70	100%
XQGAN-MSVR <sup>10P<sup>2</sup></sup>	10	2		✓	✓		$1 \times 1 \rightarrow 11 \times 11$	16384	<b>0.67</b>	100%
XQGAN-MSBR <sup>10P<sup>2</sup></sup>	10	2		✓		✓	$1 \times 1 \rightarrow 11 \times 11$	4096	0.86	100%
XQGAN-MSBR <sup>10P<sup>2</sup></sup>	10	2		✓		✓	$1 \times 1 \rightarrow 11 \times 11$	16384	0.78	100%

Table 2. Reconstruction performance comparison on ImageNet 256x256.  $|\mathcal{C}|$  denotes codebook size.  $\uparrow$  and  $\downarrow$  denote the larger the better and the smaller the better respectively. The XQGAN variants are named by MS(Multi-Scale)-{V(VQ), L(LFQ), B(BSQ)}-R<sup>N</sup>(RQ)-P<sup>P</sup>(PQ) where  $N$  and  $P$  denotes residual depth and sub-quantizer number respectively.

**PatchGAN.** PatchGAN [21] is a discriminator architecture commonly used in image tokenizers and generative adversarial networks (GANs). Instead of evaluating the entire image, it operates on smaller patches of an image. This patch-based evaluation encourages the generator to focus on producing fine-grained, localized details that appear realistic at the patch level. By modeling texture, structure, and small-scale details independently of global coherence, PatchGAN effectively guides the generator to improve the quality of individual image regions.

**StyleGAN.** StyleGAN [22] introduces a more sophisticated discriminator designed to assess image realism while preserving global semantic consistency. Its architecture emphasizes the hierarchical nature of image generation, aligning with StyleGAN’s generator that disentangles high-level attributes (e.g., pose and identity) from low-level details (e.g., texture and color). The discriminator aims to ensure that both fine details and overall structure are coherent.

**DINOv2.** DINOv2 [39], as a powerful self-supervised method for learning visual representation, also shows its effectiveness in generating images recently. By leveraging its ability to extract rich semantic features, DINOv2 can be utilized as a discriminator to evaluate the semantic consistency between real and fake images. Compared with PatchGAN [21] and StyleGAN [22], its adversarial is built upon more semantic-rich space and usually achieves a more promising result in reconstruction.

## 6.1. Tuning Method

To facilitate fintuning on pre-trained checkpoints, we support the full-parameter training, LORA [19] and frozen for both encoder and decoder.

## 6.2. Loss Function

The XQGAN is trained with composite losses including reconstruction loss  $\mathcal{L}_{recon}$ , vector quantization loss  $\mathcal{L}_{VQ}$ , adversarial loss  $\mathcal{L}_{ad}$ , Perceptual loss  $\mathcal{L}_P$ , CLIP loss  $\mathcal{L}_{clip}$  and auxiliary losses  $\mathcal{L}_{aux}$ , e.g., entropy loss:

$$\mathcal{L} = \lambda_{recon} \mathcal{L}_{recon} + \lambda_{VQ} \mathcal{L}_{VQ} + \lambda_{ad} \mathcal{L}_{ad} + \lambda_P \mathcal{L}_P + \lambda_{clip} \mathcal{L}_{clip} + \lambda_{aux} \mathcal{L}_{aux}. \quad (6)$$

Specifically, the reconstruction loss measures the  $L_2$  distance between the reconstructed image and the ground truth; vector quantization loss encourages the encoded features and its aligned codebook vectors; adversarial loss, applied from a DINO [39] discriminator trained simultaneously, ensures that the generated images are indistinguishable from real ones; perceptual loss compares high-level feature representations from a pre-trained LPIPS [79] to capture structural differences; and CLIP loss performs semantic regularization between semantic tokens and the pre-trained DINOv2 [39] features. A LeCam regularization [59] is applied to the adversarial loss to stabilize the training.

## 7. Experiments

### 7.1. Experimental Settings

We test our XQ-GAN tokenizer on the ImageNet 256x256 reconstruction and generation tasks. Additional models are trained on a subset of LAION-400M [51] (text-rich natural image dataset) and a balanced subset of IMed-361M [5] (14 categories, multimodal medical image dataset) to provide weights for the community.

The experiments are conducted on 32 NVIDIA A100 GPUs (80G) or 128 Intel Habana Gaudi HPUs (32G). For the ImageNet dataset, the training of the tokenizer takes

ID	Tokenizer	Codebook	Quant.-1	Quant.-2	rFID $\downarrow$	Generator Size	Token Length	gFID $\downarrow$
0	VAR [57]	4096	None	-	0.90	310M	680	3.30
1	XQGAN-MSR <sup>10</sup> P <sup>2</sup>	4096	DINO	None	0.80	362M	286	2.60
2	XQGAN-MSR <sup>10</sup> P <sup>2</sup>	4096	DINO	SAM	0.71	362M	286	3.46
3	XQGAN-MSBR <sup>10</sup> P <sup>2</sup>	4096	None	None	1.03	362M	286	5.83
4	XQGAN-MSBR <sup>10</sup> P <sup>2</sup>	4096	DINO	None	0.97	362M	286	3.54
5	XQGAN-MSBR <sup>10</sup> P <sup>2</sup>	4096	DINO	CLIP	0.84	362M	286	4.39
6	XQGAN-MSBR <sup>10</sup> P <sup>2</sup>	4096	DINO	SAM	0.86	362M	286	3.30
7	XQGAN-MSBR <sup>10</sup> P <sup>2</sup>	16384	DINO	SAM	0.78	310M	286	2.96

Table 3. An overall comparison of XQ-GAN on ImageNet 256x256 with different configurations. Quant.-1 and Quant.-2 denote the alignment models used in the respective quantization branches. All the generators are trained with a 10-step VAR scheme.



Figure 6. Visualization of 256  $\times$  256 image reconstruction task on (a) Imagenet, (b) LAION-400M, and (c) IMed-361M.

about 1.5-2 days depending on the specific setting. The training of the generator takes about 2 days for about 300M VAR [57] model (without flash-attention).

**Metrics.** We measure the codebook utilization rate using VAR’s implementation [57]. For reconstruction and generation, Fréchet Inception Distance (FID) [17] is utilized to evaluate the image quality.

**Implementation details.** For the XQGAN tokenizer, if there is no other specification, we follow the VQGAN training recipe of LlamaGen [55] and use the XQ-GAN-SC pipeline. We set the batch size to 1024 for all experiments. We initialize the image encoder with the weight of the DINOv2-base. We use a cosine learning rate scheduler with a warmup for 1 epoch and a start learning rate of 3e-5. We set the quantizer drop ratio to 0.1. We set  $\lambda_{clip} = 0.1$ ,  $\lambda_{recon} = \lambda_{VQ} = \lambda_P = 1$  and  $\lambda_{ad} = 0.5$ . The residual quantization of each branch shares the same codebook across scales. If quantizer dropout is applied, all branches will share the same dropout schedule. The dropout starts with a  $N_{start} = 3$  for stability issues. For the generator, we adopt VAR’s [57] GPT-2-based [42] architecture.

## 7.2. Main Results on ImageNet

We summarize our tokenizer’s performance on ImageNet reconstruction and generation benchmark of resolution 256x256 in Tab. 2 and Tab. 3 respectively.

**Reconstruction Performance on ImageNet.** To efficiently evaluate the performance of our proposed XQGAN,

we compare our method in multiple settings with prior tokenizers. As shown in Tab. 2, in tokenizers without residual quantization, our XQGAN-VP<sup>2</sup> achieves comparable results to MAGViT-v2 [74] (0.94 rFID vs. 0.90 rFID) despite using a significantly smaller codebook size (4096 vs. 262144). Notably, when the codebook size of XQGAN-VP<sup>2</sup> is increased from 4096 to 16,384, its performance improves significantly, achieving an rFID of 0.64. On the other hand, for tokenizers with residual quantization, our proposed tokenizer also demonstrates clear advantages over prior approaches. Specifically, XQGAN-MSVR<sup>10</sup>P<sup>2</sup> surpasses VAR’s tokenizer with a lower rFID (0.86 vs. 0.90) while using significantly fewer tokens (286 vs. 680). This reduction in token count effectively decreases the computational burden during generative model training, improving overall efficiency. To comprehensively evaluate the performance of our tokenizer, we introduce XQGAN-MSBR<sup>10</sup>P<sup>2</sup>, a novel variant of BSQ. With a codebook size of 16,384, this method achieves an rFID of 0.78, further highlighting the effectiveness of our approach.

**Generation Performance on ImageNet.** Benefiting from our rich-semantic tokenizer, our XQGAN further shows its superior capacity in generation. As shown in Tab. 3, we evaluate different combinations of alignment models in different quantization branches. (1) In Vector Quantization-based XQGAN, we observe that distilling DINO’s [39] and SAM’s [23] features into separate branches achieves strong performance (0.71 rFID). However, the best generative performance is obtained when the tokenizer distills only DINO’s features within a single quantization branch (2.60

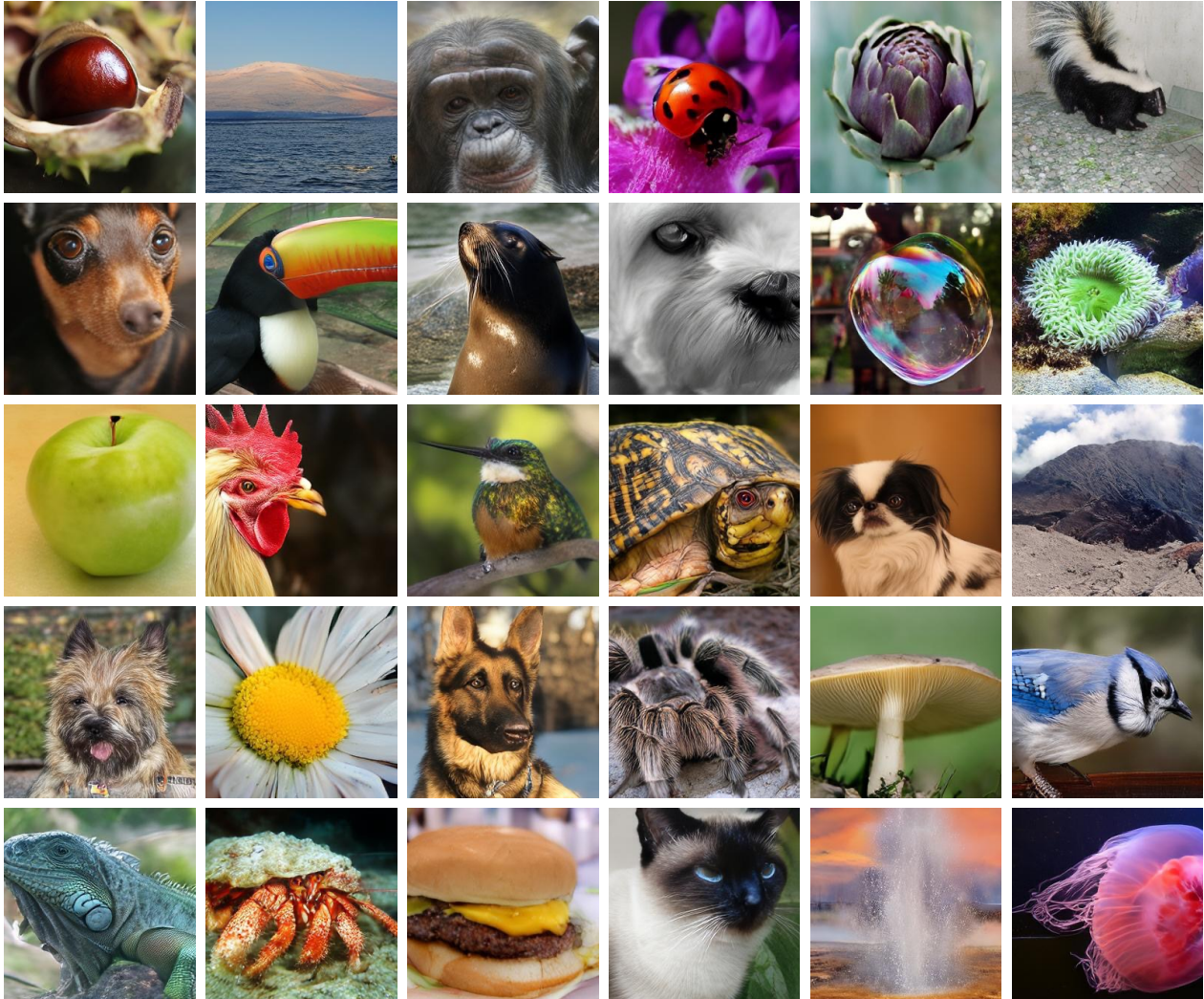


Figure 7. Visualization of  $256 \times 256$  image generation task within ImageNet classes using XQ-GAN-MSVR<sup>10P<sup>2</sup></sup> tokenizer and VAR [57] generator.

gFID with 0.80 rFID). (2) In Lookup-Free Quantization-based XQGAN, we observe that distilling DINO and SAM features into separate quantization branches achieves the best performance, with an rFID of 0.86 and a gFID of 3.30. Furthermore, XQGAN-MSBR<sup>10P<sup>2</sup></sup> demonstrates promising scalability when increasing the codebook size from 4096 to 16,384, resulting in a 0.34 gFID improvement.

### 7.3. Visualization of reconstructed images.

We present visualizations of reconstructed images from the ImageNet [7], LAION-400M [51], and IMed-361M [5] datasets to further evaluate the performance of our proposed XQGAN. As illustrated in Fig. 7, our model demonstrates consistent reconstruction quality across diverse datasets and domains, maintaining both semantic accuracy and visual fidelity.

**Visualization of generated images on ImageNet.** We demonstrate qualitative visualization of the generative model trained with XQGAN-MSVR<sup>10P<sup>2</sup></sup> as shown in Fig. 7. The classes of generated images are among the ImageNet [7] dataset with a resolution of  $256 \times 256$ .

## 8. Conclusion

In this paper, we comprehensively ablate the image reconstruction and image generation using the XQ-GAN framework. With the hierarchical quantizer design, XQ-GAN achieves state-of-the-art performance for image reconstruction, with latent tokens for both VAR and AR scheme generation. Notably, XQ-GAN is highly customizable and open-source. To facilitate the community’s use, we provide pre-trained checkpoints and support multiple fine-tuning settings.

## References

- [1] Dosovitskiy Alexey. An image is worth 16x16 words: Transformers for image recognition at scale. *arXiv preprint arXiv: 2010.11929*, 2020. 1
- [2] Alexei Baevski, Yuhao Zhou, Abdelrahman Mohamed, and Michael Auli. wav2vec 2.0: A framework for self-supervised learning of speech representations. *Advances in neural information processing systems*, 33:12449–12460, 2020. 5
- [3] Hangbo Bao, Li Dong, Songhao Piao, and Furu Wei. Beit: Bert pre-training of image transformers, 2022. 2
- [4] Huiwen Chang, Han Zhang, Lu Jiang, Ce Liu, and William T. Freeman. Maskgit: Masked generative image transformer, 2022. 2
- [5] Junlong Cheng, Bin Fu, Jin Ye, Guoan Wang, Tianbin Li, Haoyu Wang, Ruoyu Li, He Yao, Junren Chen, JingWen Li, et al. Interactive medical image segmentation: A benchmark dataset and baseline. *arXiv preprint arXiv:2411.12814*, 2024. 1, 2, 6, 8
- [6] Timothée Darcet, Maxime Oquab, Julien Mairal, and Piotr Bojanowski. Vision transformers need registers, 2023. 2
- [7] Jia Deng, Wei Dong, Richard Socher, Li-Jia Li, Kai Li, and Li Fei-Fei. Imagenet: A large-scale hierarchical image database. In *2009 IEEE conference on computer vision and pattern recognition*, pages 248–255. Ieee, 2009. 1, 2, 8
- [8] Prafulla Dhariwal and Alex Nichol. Diffusion models beat gans on image synthesis, 2021. 2
- [9] Ming Ding, Zhuoyi Yang, Wenyi Hong, Wendi Zheng, Chang Zhou, Da Yin, Junyang Lin, Xu Zou, Zhou Shao, Hongxia Yang, et al. Cogview: Mastering text-to-image generation via transformers. *Advances in neural information processing systems*, 34:19822–19835, 2021. 3
- [10] Xiaoyi Dong, Jianmin Bao, Ting Zhang, Dongdong Chen, Weiming Zhang, Lu Yuan, Dong Chen, Fang Wen, Nenghai Yu, and Baining Guo. Poco: Perceptual codebook for bert pre-training of vision transformers. In *Proceedings of the AAAI Conference on Artificial Intelligence*, pages 552–560, 2023. 2
- [11] Alexey Dosovitskiy, Lucas Beyer, Alexander Kolesnikov, Dirk Weissenborn, Xiaohua Zhai, Thomas Unterthiner, Mostafa Dehghani, Matthias Minderer, Georg Heigold, Sylvain Gelly, Jakob Uszkoreit, and Neil Houlsby. An image is worth 16x16 words: Transformers for image recognition at scale, 2021. 2
- [12] Patrick Esser, Robin Rombach, and Bjorn Ommer. Taming transformers for high-resolution image synthesis. In *Proceedings of the IEEE/CVF conference on computer vision and pattern recognition*, pages 12873–12883, 2021. 1, 2, 3, 4, 6
- [13] Oran Gafni, Adam Polyak, Oron Ashual, Shelly Sheynin, Devi Parikh, and Yaniv Taigman. Make-a-scene: Scene-based text-to-image generation with human priors. In *European Conference on Computer Vision*, pages 89–106. Springer, 2022. 3
- [14] Yuchao Gu, Xintao Wang, Yixiao Ge, Ying Shan, Xiaohu Qie, and Mike Zheng Shou. Rethinking the objectives of vector-quantized tokenizers for image synthesis, 2023. 2
- [15] Chen Hao, Wang Ze, Li Xiang, Sun Ximeng, Chen Fangyi, Liu Jiang, Wang Jindong, Raj Bhiksha, Liu Zicheng, and Barsoum Emad. Softvq-vae: Efficient 1-dimensional continuous tokenizer. *arXiv preprint arXiv*, 2024. 2, 5
- [16] Wanggui He, Siming Fu, Mushui Liu, Xierui Wang, Wenyi Xiao, Fangxun Shu, Yi Wang, Lei Zhang, Zhelun Yu, Haoyuan Li, et al. Mars: Mixture of autoregressive models for fine-grained text-to-image synthesis. *arXiv preprint arXiv:2407.07614*, 2024. 2
- [17] Martin Heusel, Hubert Ramsauer, Thomas Unterthiner, Bernhard Nessler, and Sepp Hochreiter. Gans trained by a two time-scale update rule converge to a local nash equilibrium. *Advances in Neural Information Processing Systems*, 30, 2017. 7
- [18] Geoffrey E Hinton and Ruslan R Salakhutdinov. Reducing the dimensionality of data with neural networks. *science*, 313(5786):504–507, 2006. 2
- [19] Edward J. Hu, Yelong Shen, Phillip Wallis, Zeyuan Allen-Zhu, Yuanzhi Li, Shean Wang, and Weizhu Chen. Lora: Low-rank adaptation of large language models, 2021. 1, 6
- [20] Mengqi Huang, Zhendong Mao, Zhuowei Chen, and Yongdong Zhang. Towards accurate image coding: Improved autoregressive image generation with dynamic vector quantization. In *Proceedings of the IEEE/CVF Conference on Computer Vision and Pattern Recognition*, pages 22596–22605, 2023. 2
- [21] Phillip Isola, Jun-Yan Zhu, Tinghui Zhou, and Alexei A. Efros. Image-to-image translation with conditional adversarial networks. In *Proceedings of the IEEE Conference on Computer Vision and Pattern Recognition (CVPR)*, pages 1125–1134, 2017. 1, 6
- [22] Tero Karras, Samuli Laine, and Timo Aila. A style-based generator architecture for generative adversarial networks. In *Proceedings of the IEEE/CVF Conference on Computer Vision and Pattern Recognition (CVPR)*, pages 4401–4410, 2019. 1, 6
- [23] Alexander Kirillov, Eric Mintun, Nikhila Ravi, Hanzi Mao, Chloe Rolland, Laura Gustafson, Tete Xiao, Spencer Whitehead, Alexander C. Berg, Wan-Yen Lo, Piotr Dollár, and Ross Girshick. Segment anything. *arXiv:2304.02643*, 2023. 7

[24] Rithesh Kumar, Prem Seetharaman, Alejandro Luebs, Ishaan Kumar, and Kundan Kumar. High-fidelity audio compression with improved rvqgan. *Advances in Neural Information Processing Systems*, 36, 2024. 5

[25] Doyup Lee, Chiheon Kim, Saehoon Kim, Minsu Cho, and Wook-Shin Han. Autoregressive image generation using residual quantization. In *Proceedings of the IEEE/CVF Conference on Computer Vision and Pattern Recognition*, pages 11523–11532, 2022. 2

[26] Doyup Lee, Chiheon Kim, Saehoon Kim, Minsu Cho, and Wook-Shin Han. Autoregressive image generation using residual quantization, 2022. 1, 2, 6

[27] Haopeng Li, Jinyue Yang, Kexin Wang, Xuerui Qiu, Yuhong Chou, Xin Li, and Guoqi Li. Scalable autoregressive image generation with mamba. *arXiv preprint arXiv:2408.12245*, 2024. 2

[28] Tianhong Li, Huiwen Chang, Shlok Kumar Mishra, Han Zhang, Dina Katabi, and Dilip Krishnan. Mage: Masked generative encoder to unify representation learning and image synthesis, 2023. 2

[29] Tianhong Li, Yonglong Tian, He Li, Mingyang Deng, and Kaiming He. Autoregressive image generation without vector quantization, 2024. 2

[30] Xiang Li, Kai Qiu, Hao Chen, Jason Kuen, Jiuxiang Gu, Bhiksha Raj, and Zhe Lin. Imagefolder: Autoregressive image generation with folded tokens. *arXiv preprint arXiv:2410.01756*, 2024. 1, 2, 3, 5

[31] Xiang Li, Kai Qiu, Hao Chen, Jason Kuen, Zhe Lin, Rita Singh, and Bhiksha Raj. Controlvar: Exploring controllable visual autoregressive modeling. *arXiv preprint arXiv:2406.09750*, 2024. 1, 2

[32] Dongyang Liu, Shitian Zhao, Le Zhuo, Weifeng Lin, Yu Qiao, Hongsheng Li, and Peng Gao. Lumina-mgpt: Illuminate flexible photorealistic text-to-image generation with multimodal generative pretraining. *arXiv preprint arXiv:2408.02657*, 2024. 2

[33] Zhuoyan Luo, Fengyuan Shi, Yixiao Ge, Yujiu Yang, Limin Wang, and Ying Shan. Openmagvit2: An open-source project toward democratizing auto-regressive visual generation. *arXiv preprint arXiv:2409.04410*, 2024. 2

[34] Fabian Mentzer, David Minnen, Eirikur Agustsson, and Michael Tschannen. Finite scalar quantization: Vq-vae made simple, 2023. 2

[35] David Mizrahi, Roman Bachmann, Oguzhan Kar, Teresa Yeo, Mingfei Gao, Afshin Dehghan, and Amir Zamir. 4m: Massively multimodal masked modeling. *Advances in Neural Information Processing Systems*, 36, 2024. 2

[36] Alex Nichol and Prafulla Dhariwal. Improved denoising diffusion probabilistic models, 2021. 2

[37] Alex Nichol, Prafulla Dhariwal, Aditya Ramesh, Pranav Shyam, Pamela Mishkin, Bob McGrew, Ilya Sutskever, and Mark Chen. Glide: Towards photorealistic image generation and editing with text-guided diffusion models. *arXiv preprint arXiv:2112.10741*, 2021. 3

[38] J Ning, C Li, Z Zhang, Z Geng, Q Dai, K He, and H Hu. All in tokens: Unifying output space of visual tasks via soft token. arxiv 2023. *arXiv preprint arXiv:2301.02229*. 2

[39] Maxime Oquab, Timothée Darctet, Theo Moutakanni, Huy V. Vo, Marc Szafraniec, Vasil Khalidov, Pierre Fernandez, Daniel Haziza, Francisco Massa, Alaaeldin El-Nouby, Russell Howes, Po-Yao Huang, Hu Xu, Vasu Sharma, Shang-Wen Li, Wojciech Galuba, Mike Rabbat, Mido Assran, Nicolas Ballas, Gabriel Synnaeve, Ishan Misra, Herve Jegou, Julien Mairal, Patrick Labatut, Armand Joulin, and Piotr Bojanowski. Dinov2: Learning robust visual features without supervision, 2023. 2, 5, 6, 7

[40] William Peebles and Saining Xie. Scalable diffusion models with transformers, 2023. 3

[41] Zhiliang Peng, Li Dong, Hangbo Bao, Qixiang Ye, and Furu Wei. Beit v2: Masked image modeling with vector-quantized visual tokenizers, 2022. 2

[42] Alec Radford, Jeffrey Wu, Rewon Child, David Luan, Dario Amodei, Ilya Sutskever, et al. Language models are unsupervised multitask learners. *OpenAI blog*, 1(8):9, 2019. 7

[43] Alec Radford, Jong Wook Kim, Chris Hallacy, Aditya Ramesh, Gabriel Goh, Sandhini Agarwal, Girish Sastry, Amanda Askell, Pamela Mishkin, Jack Clark, et al. Learning transferable visual models from natural language supervision. In *International conference on machine learning*, pages 8748–8763. PMLR, 2021. 2, 5

[44] Aditya Ramesh, Mikhail Pavlov, Gabriel Goh, Scott Gray, Chelsea Voss, Alec Radford, Mark Chen, and Ilya Sutskever. Zero-shot text-to-image generation. In *International conference on machine learning*, pages 8821–8831. Pmlr, 2021. 3

[45] Ali Razavi, Aaron Van den Oord, and Oriol Vinyals. Generating diverse high-fidelity images with vq-vae-2. *Advances in neural information processing systems*, 32, 2019. 2

[46] Ali Razavi, Aaron van den Oord, and Oriol Vinyals. Generating diverse high-fidelity images with vq-vae-2, 2019. 2

[47] Robin Rombach, Andreas Blattmann, Dominik Lorenz, Patrick Esser, and Björn Ommer. High-resolution image synthesis with latent diffusion models. In *Proceedings of the IEEE/CVF conference on computer vision and pattern recognition*, pages 10684–10695, 2022. 1, 3

[48] Robin Rombach, Andreas Blattmann, Dominik Lorenz, Patrick Esser, and Björn Ommer. High-resolution image synthesis with latent diffusion models, 2022. 3

[49] Olaf Ronneberger, Philipp Fischer, and Thomas Brox. U-net: Convolutional networks for biomedical image segmentation. In *Medical image computing and computer-assisted intervention–MICCAI 2015: 18th international conference, Munich, Germany, October 5–9, 2015, proceedings, part III* 18, pages 234–241. Springer, 2015. 2

[50] Chitwan Saharia, William Chan, Saurabh Saxena, Lala Li, Jay Whang, Emily L Denton, Kamvar Ghasemipour, Raphael Gontijo Lopes, Burcu Karagol Ayan, Tim Salimans, et al. Photorealistic text-to-image diffusion models with deep language understanding. *Advances in neural information processing systems*, 35:36479–36494, 2022. 3

[51] Christoph Schuhmann, Richard Vencu, Romain Beaumont, Robert Kaczmarczyk, Clayton Mullis, Aarush Katta, Theo Coombes, Jenia Jitsev, and Aran Komatsuzaki. Laion-400m: Open dataset of clip-filtered 400 million image-text pairs. *arXiv preprint arXiv:2111.02114*, 2021. 1, 2, 6, 8

[52] Jie Shi, Chenfei Wu, Jian Liang, Xiang Liu, and Nan Duan. Divae: Photorealistic images synthesis with denoising diffusion decoder, 2022. 2

[53] Jascha Sohl-Dickstein, Eric A. Weiss, Niru Maheswaranathan, and Surya Ganguli. Deep unsupervised learning using nonequilibrium thermodynamics, 2015. 2

[54] Jiaming Song, Chenlin Meng, and Stefano Ermon. Denoising diffusion implicit models, 2022. 3

[55] Peize Sun, Yi Jiang, Shoufa Chen, Shilong Zhang, Bingyue Peng, Ping Luo, and Zehuan Yuan. Autoregressive model beats diffusion: Llama for scalable image generation. *arXiv preprint arXiv:2406.06525*, 2024. 1, 2, 7

[56] Yuhta Takida, Yukara Ikemiya, Takashi Shibuya, Kazuki Shimada, Woosung Choi, Chieh-Hsin Lai, Naoki Murata, Toshimitsu Uesaka, Kengo Uchida, Wei-Hsiang Liao, et al. Hq-vae: Hierarchical discrete representation learning with variational bayes. *arXiv preprint arXiv:2401.00365*, 2023. 2

[57] Keyu Tian, Yi Jiang, Zehuan Yuan, Bingyue Peng, and Liwei Wang. Visual autoregressive modeling: Scalable image generation via next-scale prediction, 2024. 1, 2, 4, 5, 6, 7, 8

[58] Hugo Touvron, Thibaut Lavrille, Gautier Izacard, Xavier Martinet, Marie-Anne Lachaux, Timothée Lacroix, Baptiste Rozière, Naman Goyal, Eric Hambro, Faisal Azhar, Aurelien Rodriguez, Armand Joulin, Edouard Grave, and Guillaume Lample. Llama: Open and efficient foundation language models, 2023. 2

[59] Hung-Yu Tseng, Lu Jiang, Ce Liu, Ming-Hsuan Yang, and Weilong Yang. Regularizing generative adversarial networks under limited data, 2021. 6

[60] Arash Vahdat, Karsten Kreis, and Jan Kautz. Score-based generative modeling in latent space, 2021. 3

[61] Aaron Van den Oord, Nal Kalchbrenner, Lasse Espeholt, Oriol Vinyals, Alex Graves, et al. Conditional image generation with pixelcnn decoders. *Advances in neural information processing systems*, 29, 2016. 2

[62] Aaron Van Den Oord, Oriol Vinyals, et al. Neural discrete representation learning. *Advances in neural information processing systems*, 30, 2017. 1, 2, 3

[63] Ashish Vaswani, Noam Shazeer, Niki Parmar, Jakob Uszkoreit, Llion Jones, Aidan N. Gomez, Łukasz Kaiser, and Illia Polosukhin. Attention is all you need, 2023. 2

[64] Pascal Vincent, Hugo Larochelle, Yoshua Bengio, and Pierre-Antoine Manzagol. Extracting and composing robust features with denoising autoencoders. In *Proceedings of the 25th international conference on Machine learning*, pages 1096–1103, 2008. 2

[65] Huiyu Wang, Yukun Zhu, Hartwig Adam, Alan Yuille, and Liang-Chieh Chen. Max-deeplab: End-to-end panoptic segmentation with mask transformers, 2021. 2

[66] Mark Weber, Lijun Yu, Qihang Yu, Xueqing Deng, Xiaohui Shen, Daniel Cremers, and Liang-Chieh Chen. Maskbit: Embedding-free image generation via bit tokens. *arXiv preprint arXiv:2409.16211*, 2024. 1, 2

[67] Yecheng Wu, Zhuoyang Zhang, Junyu Chen, Haotian Tang, Dacheng Li, Yunhao Fang, Ligeng Zhu, Enze Xie, Hongxu Yin, Li Yi, et al. Vila-u: a unified foundation model integrating visual understanding and generation. *arXiv preprint arXiv:2409.04429*, 2024. 1, 2, 5

[68] Jinheng Xie, Weijia Mao, Zechen Bai, David Junhao Zhang, Weihao Wang, Kevin Qinghong Lin, Yuchao Gu, Zhiping Chen, Zhenheng Yang, and Mike Zheng Shou. Show-o: One single transformer to unify multimodal understanding and generation. *arXiv preprint arXiv:2408.12528*, 2024. 2

[69] Lihe Yang, Bingyi Kang, Zilong Huang, Xiaogang Xu, Jiashi Feng, and Hengshuang Zhao. Depth anything: Unleashing the power of large-scale unlabeled data. In *Proceedings of the IEEE/CVF Conference on Computer Vision and Pattern Recognition*, pages 10371–10381, 2024. 2

[70] Jiahui Yu, Xin Li, Jing Yu Koh, Han Zhang, Ruoming Pang, James Qin, Alexander Ku, Yuanzhong Xu, Jason Baldridge, and Yonghui Wu. Vector-quantized

image modeling with improved vqgan. *arXiv preprint arXiv:2110.04627*, 2021. 2, 6

[71] Lijun Yu, Yong Cheng, Kihyuk Sohn, José Lezama, Han Zhang, Huiwen Chang, Alexander G Hauptmann, Ming-Hsuan Yang, Yuan Hao, Irfan Essa, et al. Magvit: Masked generative video transformer. In *Proceedings of the IEEE/CVF Conference on Computer Vision and Pattern Recognition*, pages 10459–10469, 2023. 2, 5

[72] Lijun Yu, José Lezama, Nitesh B. Gundavarapu, Luca Versari, Kihyuk Sohn, David Minnen, Yong Cheng, Agrim Gupta, Xiuye Gu, Alexander G. Hauptmann, Boqing Gong, Ming-Hsuan Yang, Irfan Essa, David A. Ross, and Lu Jiang. Language model beats diffusion – tokenizer is key to visual generation, 2023.

[73] Lijun Yu, Yong Cheng, Zhiruo Wang, Vivek Kumar, Wolfgang Macherey, Yanping Huang, David Ross, Irfan Essa, Yonatan Bisk, Ming-Hsuan Yang, et al. Spae: Semantic pyramid autoencoder for multimodal generation with frozen llms. *Advances in Neural Information Processing Systems*, 36, 2024. 1, 2

[74] Lijun Yu, Jose Lezama, Nitesh Bharadwaj Gundavarapu, Luca Versari, Kihyuk Sohn, David Minnen, Yong Cheng, Agrim Gupta, Xiuye Gu, Alexander G Hauptmann, Boqing Gong, Ming-Hsuan Yang, Irfan Essa, David A Ross, and Lu Jiang. Language model beats diffusion - tokenizer is key to visual generation. In *The Twelfth International Conference on Learning Representations*, 2024. 1, 2, 6, 7

[75] Qihang Yu, Mark Weber, Xueqing Deng, Xiaohui Shen, Daniel Cremers, and Liang-Chieh Chen. An image is worth 32 tokens for reconstruction and generation. *arxiv: 2406.07550*, 2024. 2

[76] Qihang Yu, Mark Weber, Xueqing Deng, Xiaohui Shen, Daniel Cremers, and Liang-Chieh Chen. An image is worth 32 tokens for reconstruction and generation, 2024. 1

[77] Sihyun Yu, Sangkyung Kwak, Huiwon Jang, Jongheon Jeong, Jonathan Huang, Jinwoo Shin, and Saining Xie. Representation alignment for generation: Training diffusion transformers is easier than you think. *arXiv preprint arXiv:2410.06940*, 2024. 2

[78] Neil Zeghidour, Alejandro Luebs, Ahmed Omran, Jan Skoglund, and Marco Tagliasacchi. Soundstream: An end-to-end neural audio codec. *IEEE/ACM Transactions on Audio, Speech, and Language Processing*, 30: 495–507, 2021. 5

[79] Richard Zhang, Phillip Isola, Alexei A. Efros, Eli Shechtman, and Oliver Wang. The unreasonable effectiveness of deep features as a perceptual metric, 2018. 6

[80] Yue Zhao, Yuanjun Xiong, and Philipp Krähenbühl. Image and video tokenization with binary spherical quantization. *arXiv preprint arXiv:2406.07548*, 2024. 1, 2

[81] Chuanxia Zheng, Long Tung Vuong, Jianfei Cai, and Dinh Phung. Movq: Modulating quantized vectors for high-fidelity image generation, 2022. 2

[82] Chunting Zhou, Lili Yu, Arun Babu, Kushal Tirumala, Michihiro Yasunaga, Leonid Shamis, Jacob Kahn, Xuezhe Ma, Luke Zettlemoyer, and Omer Levy. Transfusion: Predict the next token and diffuse images with one multi-modal model. *arXiv preprint arXiv:2408.11039*, 2024. 2

[83] Lei Zhu, Fangyun Wei, Yanye Lu, and Dong Chen. Scaling the codebook size of vqgan to 100,000 with a utilization rate of 99%. *arXiv preprint arXiv:2406.11837*, 2024. 2

[84] X Zhu, W Su, L Lu, B Li, X Wang, and J Dai. Deformable detr: Deformable transformers for end-to-end object detection. *arxiv 2020*. *arXiv preprint arXiv:2010.04159*, 2010. 2

[85] Yongxin Zhu, Bocheng Li, Yifei Xin, and Linli Xu. Addressing representation collapse in vector quantized models with one linear layer. *arXiv preprint arXiv:2411.02038*, 2024. 2

[86] Yongxin Zhu, Bocheng Li, Hang Zhang, Xin Li, Linli Xu, and Lidong Bing. Stabilize the latent space for image autoregressive modeling: A unified perspective. *arXiv preprint arXiv:2410.12490*, 2024. 2